

Light-Induced Retinal Changes Observed with High-Resolution Autofluorescence Imaging of the Retinal Pigment Epithelium

Jessica I. W. Morgan,¹ Jennifer J. Hunter,¹ Benjamin Masella,¹ Robert Wolfe,¹ Daniel C. Gray,¹ William H. Merigan,¹ François C. Delori,² and David R. Williams¹

PURPOSE. Autofluorescence fundus imaging using an adaptive optics scanning laser ophthalmoscope (AOSLO) allows for imaging of individual retinal pigment epithelial (RPE) cells in vivo. In this study, the potential of retinal damage was investigated by using radiant exposure levels that are 2 to 150 times those used for routine imaging.

METHODS. Macaque retinas were imaged in vivo with a fluorescence AOSLO. The retina was exposed to 568- or 830-nm light for 15 minutes at various intensities over a square $\frac{1}{2}^\circ$ per side. Pre- and immediate postexposure images of the photoreceptors and RPE cells were taken over a 2° field. Long-term AOSLO imaging was performed intermittently from 5 to 165 days after exposure. Exposures delivered over a uniform field were also investigated.

RESULTS. Exposures to 568-nm light caused an immediate decrease in autofluorescence of RPE cells. Follow-up imaging revealed either full recovery of autofluorescence or long-term damage in the RPE cells at the exposure. The outcomes of AOSLO exposures and uniform field exposures of equal average power were not significantly different. No effects from 830-nm exposures were observed.

CONCLUSIONS. The study revealed a novel change in RPE autofluorescence induced by 568-nm light exposure. Retinal damage occurred as a direct result of total average power, independent of the light-delivery method. Because the exposures were near or below permissible levels in laser safety standards, these results suggest that caution should be used with exposure of the retina to visible light and that the safety standards should be re-evaluated for these exposure conditions. (*Invest Ophthalmol Vis Sci.* 2008;49:3715-3729) DOI:10.1167/iovs.07-1430

Since the invention of the laser, damage studies have become increasingly important for understanding the safety of accidental and prescribed retinal light exposures. For example,

it is essential in procedures such as ophthalmoscopic examination or intraocular surgery to identify damage thresholds so that light exposures are a minimal risk to retinal health. Therefore, the effects of various retinal light exposures and damage mechanisms have been studied¹⁻⁴ and safety standards have been implemented to reduce the risk of ocular damage.⁵⁻⁸

Depending on exposure wavelength and duration, retinal damage can occur by one of three mechanisms: thermal, photochemical, or mechanical effects.⁹⁻¹¹ Thermal damage is thought to occur when the temperature of the retina rises 10° above its ambient temperature.^{1,9,12} Photochemical effects cause retinal damage when the incoming light interacts with molecules to cause a chemical change; molecules that could elicit photochemical effects in the retina include receptor photopigments, retinal pigment epithelial (RPE) melanin granules, or RPE lipofuscin granules.⁹ Light exposures that cause damage by thermal mechanisms include exposures to visible and near-infrared light; photochemical effects occur with exposures to visible and ultraviolet light.^{1,5} Retinal damage from mechanical effects result from the formation of microbubbles, which develop from microsecond exposures⁴; exposures in this regimen are outside of the scope of the present study.

Funduscopy examination and fluorescein angiography (FA) have been used in many studies as endpoints for detecting retinal damage,^{1,13} electroretinogram^{14,15} and histology outcome measures^{2,16} have been used in others. Nevertheless, new imaging modalities have arisen to allow for additional metrics to determine retinal health. One such technique is lipofuscin autofluorescence (AF) imaging of the RPE.^{17,18} Lipofuscin consists of a mixture of pigments, including A2E, isomers of A2E and all-*trans*-retinal dimer.¹⁹⁻²¹ It accumulates naturally in the RPE cells and thus allows investigators to study the retina by using fluorescence imaging techniques.^{19,22,23} Lipofuscin AF has allowed the RPE layer of the retina to be imaged in both normal and diseased eyes in vivo.^{17,18,24}

Further advances in ophthalmoscopy include the combination of adaptive optics (AO) with the flood-illuminated ophthalmoscope,^{25,26} the scanning laser ophthalmoscope (SLO),^{27,28} and optical coherence tomography (OCT).²⁹⁻³¹ AO imaging involves measuring the higher-order optical aberrations in the eye with a wavefront sensor and correcting these aberrations with a wavefront corrector, typically a deformable mirror. The improvements in resolution and contrast afforded by adaptive optics ophthalmoscopy have made possible in vivo imaging of microscopic retinal features, including individual cone photoreceptors,^{25,26,32-35} retinal pigment epithelial (RPE) cells (Morgan JIW, et al. *IOVS* 2007;48:ARVO E-Abstract 1953),^{28,36} ganglion cells,²⁸ leukocyte cells,³⁷ and the lamina cribrosa of the optic disc.³⁸ We have shown that the combination of AF techniques with an adaptive optics scanning laser ophthalmoscope (AOSLO) yields images of the complete RPE cell mosaic in the living eye (Morgan JIW, et al. *IOVS* 2007;48:ARVO E-Abstract 1953).²⁸

In the present study, we explored the potential for light-induced retinal damage to optimize the parameters, including

From the ¹University of Rochester, Center for Visual Science, Rochester, New York; and ²Schepens Eye Research Institute, Biomedical Physics, Boston, Massachusetts.

Supported by the National Institutes of Health, Bethesda, Maryland (EY014375, EY01319, and EY07125); Bausch and Lomb; Research to Prevent Blindness; and by the National Science Foundation Science and Technology Center for Adaptive Optics (Santa Cruz, CA), managed by the University of California at Santa Cruz (cooperative agreement no. AST-9876783).

Submitted for publication November 6, 2007; revised February 14, 2008; accepted June 4, 2008.

Disclosure: **J.I.W. Morgan**, P; **J.J. Hunter**, None; **B. Masella**, None; **R. Wolfe**, None; **D.C. Gray**, Optos (E), P; **W.H. Merigan**, None; **F.C. Delori**, None; **D.R. Williams**, Bausch and Lomb (F, C), Optos (C), P

The publication costs of this article were defrayed in part by page charge payment. This article must therefore be marked "advertisement" in accordance with 18 U.S.C. §1734 solely to indicate this fact.

Corresponding author: Jessica I. W. Morgan, University of Rochester, Meliora 274, Rochester, NY 14627; jmorgan@cvs.rochester.edu.

TABLE 1. Animals

Macaque Number	Species	Age (y)	Sex	Eye	Axial Length (mm)
320	<i>Macaca fascicularis</i>	8	M	OD	17.85
620	<i>Macaca fascicularis</i>	3	M	OS	18.07
903	<i>Macaca nemestrina</i>	11	M	OD	20.97
				OS	20.95

exposure size and duration, of routine AF imaging of the RPE mosaic. We examined the effects of light exposure on the macaque retina in vivo by using AOSLO AF RPE imaging and AOSLO photoreceptor imaging, as well as color and fluorescein photography. Although AF imaging has been used to detect light-induced retinal damage, those studies have been confined to patients undergoing laser treatment.³⁹⁻⁴¹ To the best of our knowledge, AF imaging has not been used in any study as an endpoint to study light damage near threshold exposure levels. In addition, retinal damage has been assessed with high-resolution AO imaging techniques. We used both AO and AF imaging to provide high-resolution in vivo observations of a novel change in RPE cell AF as a result of light exposure as well as a high-resolution outcome measure for retinal damage in the photoreceptor and RPE cell mosaics. The ability to detect these changes in retinal AF with the AOSLO may provide a more sensitive endpoint for determining the safety of light exposures.

Currently, several internationally recognized standards⁵⁻⁸ including the American National Standards Institute (ANSI) Standard for the Safe Use of Lasers establish safe light exposure conditions and provide maximum permissible exposure (MPE) limits dependent on specific conditions of light exposures including wavelength, exposure duration, and size of the irradiated retinal area.^{5,42} The exposure limits recommended by the different standards are nearly identical. The exposures tested in the present study are near or below the MPE limits set forth by these standards, but our results show retinal damage as a result of exposures previously thought to be safe. This suggests that these safety standards should be changed for the type of exposures used in this study to reflect more conservative exposure limits.

METHODS

Macaque Preparation

Four eyes of three macaques were used for these experiments only. Table 1 shows the parameters for each macaque. During AOSLO imaging, the macaque was anesthetized with isoflurane (1.0%-3.0%), body temperature was monitored, and pupils were dilated and cyclopleged with phenylephrine hydrochloride (2.5%) and tropicamide (1%). A lid speculum held the imaged eye open, and a rigid gas-permeable contact lens was used to protect the cornea.⁴³ The animal's head and pupil of the eye were aligned with the imaging system by a head prostration mount and a three-axis translation stage (Velmex, Bloomfield, NY) as previously described.²⁸ In addition to several AOSLO imaging sessions, fundus photography and FA were performed on each monkey. Axial length was measured in the eyes of each animal by averaging 10 measurements made by B-scan ultrasound. Axial lengths were used to determine the scale of the retinal images by linearly scaling the LeGrand model eye.⁴⁴ The focal lengths were approximated by dividing the axial lengths by 1.4 (the ratio of the axial length to the distance between the nodal point and the retina in the LeGrand eye model).⁴⁴ A focal length of 15 mm was used for all calculations of the radiant exposures and the ANSI MPEs. The study procedures were in compliance with the ARVO Statement for the Use of Animals in Ophthalmic and Vision Research. The University of Rochester review board approved all experiments.

Autofluorescence Imaging of the RPE Cells

The fluorescence AOSLO used in this experiment has been described.²⁸ For fluorescence imaging, the AOSLO illuminates the retina with three lasers simultaneously. The AOSLO consists of an adjustable scanning system with a variable 0.5° to 3.5° field of view, an AO system (a Shack-Hartmann wavefront sensor, a deformable mirror [144-actuator MEMS; Boston Micromachines; Watertown, MA], and a laser beacon), two imaging lasers, and two detectors for simultaneous reflectance and fluorescence imaging.

Three lasers were simultaneously scanned across the retinal area—568-nm light from an AR/KR tunable laser for the AF excitation, 830-nm light from a laser diode for reflectance imaging, and 904-nm light from a laser diode for wavefront sensing. A reflectance movie and an AF movie were recorded simultaneously. The AF movies were taken by exciting the retina with the 568-nm light and collecting the emission over a 40-nm bandwidth centered at 624 nm for approximately 60 seconds or less (Morgan JIW, et al. *IOVS* 2007;48:ARVO E-Abstract 1953).²⁸ To correct for motion of the eye during this time, multiple reflectance images were registered, shifted, and averaged together. The movement correction associated with each frame in the reflectance movie was then applied to the simultaneously recorded AF frame. Using this method as previously described (Morgan JIW, et al. *IOVS* 2007;48:ARVO E-Abstract 1953),²⁸ multiple AF frames were averaged and images of the RPE mosaic were obtained. Each averaged image consists of 1300 individual frames.

Laser Modulation

The AOSLO operates with a fast horizontal galvanometer scanner (15.537 kHz) and a slow vertical solenoid scanner (27.26 Hz or frame/sec) where 512 raster lines are used for imaging. Under normal conditions of operation, the 568-nm laser is switched off (1) during the return beam (between each horizontal scan used for imaging and thus 50% of the time), (2) at the edges of each horizontal scan for a total of 18% of the time^{27,28} (during the changes in direction of the beam), and (3) during the flyback of the slow scanner at the end of each frame for 10% of the time. Thus, the laser is on for 37% of the total imaging time, giving an ON ratio of $0.50 \cdot 0.82 \cdot 0.90 = 0.37$. If the average power measured at the pupil is E, then the instantaneous power and the power of the beam scanning the retina is E divided by the ON ratio. To increase the average power in some exposures, we removed all blanking (1, 2, and 3), yielding an ON-ratio of 1.00, or we removed partial blanking (1 and 3), yielding an ON ratio of 0.82. The 830- and 904-nm lasers always had an ON ratio of 1.00.

Light Exposures

Four sets of light exposures were delivered to the retina. In experiments 1, 2, and 4 all three lasers were used simultaneously during the exposures. In experiment 3, only the 830- and 904-nm lasers were used. For each exposure condition, the experimental protocol was as follows: An image of the RPE cells and cone photoreceptors was taken at a given location. The retina was then exposed to a prescribed amount of light for 15 minutes over a smaller field of view than that used for the pre-exposure image. During the exposure, eye motion was monitored with the AOSLO and the retina was stabilized by manually adjusting the macaque's head position to cancel any eye movements except the pulsing from the heartbeat, which was less than approximately 0.1° in any direction. If the eye motion could not

be stabilized because of large drifts, the exposure location was abandoned, and a new exposure location was found. Immediately after each exposure, the scanners were set to the original field size, and a postexposure image of the same area as the pre-exposure image was taken of the RPE cells and cone photoreceptors. Thus, the immediate postexposure image shows both retinal area exposed to the light and surrounding retinal area excluded from the exposure. Additional images of the RPE cells and cone photoreceptors were taken at the same location and field size 5 to 9 days after exposure and were followed intermittently for up to 165 days. Preimages for each exposure did not overlap with each other and each exposure location was used only once. All exposures were contained within the vascular arcade.

Pre- and postexposure images were recorded over a 2° field and an exposure duration of approximately 60 seconds or less, with average powers of either 20 μW (ON-ratio = 0.37; instantaneous power, 55 μW) or 50 μW (ON ratio = 1.00; instantaneous power, 50 μW) of 568 nm for AF imaging, 55 to 90 μW of 904 nm for wavefront sensing, and 200 to 250 μW of 830 nm for reflectance imaging. The same powers were used for wavefront sensing and for reflectance imaging during the exposure. The power of all light entering the cornea was measured using a power meter with a silicon detector (power meter model 1930-C, detector model Phto-918-SL; Newport Corporation, Irvine, CA). The power meter and detector have an accuracy of $\pm 1\%$ and were calibrated prior to the experiments.

Experiment 1: $\frac{1}{2}^\circ$ 15-minute 568-nm Exposures.

Twelve exposures were delivered by the AOSLO over different square retinal areas, $\frac{1}{2}^\circ$ in visual angle per side ($\sim 120 \mu\text{m}$ per side), with the 568-nm laser at average powers of 3 ($n = 1$), 40 ($n = 2$), 47 ($n = 1$), 55 ($n = 3$), 140 ($n = 1$), and 150 ($n = 4$) μW . All exposures were obtained with no blanking (ON ratio = 1.00), except for the 47 and 55 μW cases in which the normal mode of operation was used (ON ratio = 0.37; thus, the instantaneous laser power on the retina was 140 and 150 μW , respectively). Pre- and postexposure images of the RPE cells and photoreceptors were taken over a square area 2° in visual angle per side.

Experiment 2: 2° 15-minute 568-nm Exposures. Seven different exposures were performed over a square area 2° in visual angle per side with the 568-nm laser at an average power of 88 μW (ON ratio = 0.82, instantaneous laser power of 110 μW). Pre- and postimaging of the RPE was performed over a square area 3.5° in visual angle per side.

Experiment 3: $\frac{1}{2}^\circ$ 15-minute 830-nm Exposures. Six exposures were made over a square area $\frac{1}{2}^\circ$ in visual angle per side with the 830-nm laser at average power of 1.6 mW (the highest power available in our system; ON ratio = 1.00). The 568-nm light was not used to illuminate the retina during the 15-minute exposure. Pre- and postexposure images were acquired over a square area 2° in visual angle per side.

Experiment 4: Alternate Light Delivery Methods. Experiment 4 tested the effects of 568-nm light with two alternative light-delivery methods in addition to the AOSLO. Because the AOSLO has not been used in light damage studies, nor is the specific case of the AOSLO described in the light safety standards, it is important to determine whether the observed retinal damage is caused by the method of exposure or the total energy of the exposure.

For one alternate method, light was delivered through the AOSLO without AO, to test whether an aberrant scanning spot would give the same results as a diffraction-limited scanning spot. Trial lenses were used to best correct defocus and astigmatism, and higher-order aberrations were left uncorrected. Seven different exposures were performed over a square area $\frac{1}{2}^\circ$ in visual angle per side with the 568-nm laser at average powers of 47 ($n = 1$, ON ratio = 0.37), 55 ($n = 3$, ON ratio = 0.37), and 150 ($n = 3$, ON ratio = 1.00) μW .

In the second method, the retina was uniformly exposed, with no scanning, by using a Maxwellian illumination system to test whether a constant, uniform exposure would give the same results as an exposure scanned over the same size field with equivalent average powers.

A beam expander was inserted in front of the AR/KR 568-nm laser source to illuminate uniformly a square area of the retina $\frac{1}{2}^\circ$ in visual angle per side. Seven exposures were made with the 568-nm laser as a uniform source with average powers of 47 ($n = 1$), 55 ($n = 3$), and 150 ($n = 3$) μW . The 904- and 830-nm light was still delivered to the retina through the AOSLO and was used for wavefront sensing, reflectance imaging, and eye motion monitoring, as described earlier.

Quantification of the AF Intensity Decrease

Pre- and postexposure images at each location were aligned and cropped so that each image included the same retinal area. The exposure site was identified within each retinal location studied. To reduce any effect of residual motion during the exposure, a region of the image surrounding the edge of the exposure site was excluded from the analysis. The excluded region extended from 0.06° inside each edge of the exposure to 0.10° outside each edge. The mean AF intensity inside and outside the exposure site was then calculated over the remaining area and the ratio of inside to outside mean AF intensity was determined for each pre- and postexposure image. To account for nonuniformities in the AF spatial distribution, each postexposure AF ratio was divided by the pre-exposure ratio. Thus, any retinal features causing a local difference in AF intensity were normalized. This normalized ratio represents the relative change in AF at the site of the exposure. We will call it the AF ratio. Using the AF ratio does not alter the basic interpretations of the raw data, but rather provides a metric normalized in both space and time for quantifying changes in the AF intensity.

Normalized AF ratios were averaged for exposures of the same average power. When appropriate, paired or unpaired *t*-tests were performed to test for the significance of changes in the calculated AF ratios. Those differences with $P < 0.05$ are considered significant. In some cases, three comparisons were made among the data involved; hence, with a Bonferroni correction for multiple comparisons, $P < 0.017$ was deemed significant.

RESULTS

Table 2 summarizes the results of the exposures in experiments 1, 2, and 4. The table shows the exposures in which damage was observed using AOSLO AF imaging, AOSLO photoreceptor imaging, and color and fluorescein angiogram (FA) photography. The AF ratio is also given immediately after exposure.

Long-term Retinal Damage: Experiment 1

Experiment 1 tested the susceptibility of the retina to different amounts of 568-nm light. Figure 1 shows the results in two retinal locations: one exposed to 150 μW and the other to 55 μW , both at 568-nm light for 15 minutes. The pre-exposure AF images (Figs. 1a, 1g) showed the RPE cell mosaics. As previously described (Morgan JIW, et al. *IOVS* 2007;48:ARVO E-Abstract 1953),²⁸ the dark center of each RPE cell is the nucleus of the RPE cell, and the bright fluorescent ring depicts the edge of the cell where lipofuscin has accumulated in the cytoplasm. The AF images immediately after exposure (Figs. 1b, 1h) showed a decrease in AF at the site of the exposure. However, no structural change in the RPE cells appeared; each RPE cell was seen in the same location as in the pre-exposure image. Table 2 gives the AF ratios immediately after exposure. The 55- and 150- μW exposures showed a significant decrease in AF immediately after exposure compared to before exposure (55 μW : $t(2) = 12.983$, $P = 0.0059$, 150 μW : $t(3) = 15.037$, $P = 0.0006$). Compared to the 55- μW exposures, the 150- μW exposures had a significantly larger effect ($t(5) = 3.451$, $P = 0.018$). No changes in the near infrared reflectance images were observed immediately after exposure (Figs. 1e, 1k).

TABLE 2. AF Ratio and Permanent Postexposure Damage (1/2°, 900 s)

Experiment Number	Macaques Used	Average Power (μW)	Radiant Exposure (J/cm^2)	AF-Ratio Immediately Postexposure	Permanent Damage*			
					RPE	Photoreceptor	Color	FA
1	320,903	150	788	0.58 ± 0.03	4/4	4/4	4/4	4/4
4 (Uniform)	320,903	150	788	0.51 ± 0.03	3/3	3/3	3/3	2/3
4 (No AO)	320,903	150	788	0.58 ± 0.03	3/3	3/3	3/3	3/3
1	903	140	735	0.70	1/1	1/1	1/1	1/1
1	620,903	55	289	0.71 ± 0.02	3/3	0/3	3/3	2/3
4 (Uniform)	620,903	55	289	0.58 ± 0.10	3/3	1/3	2/2†	2/2†
4 (No AO)	620,903	55	289	0.68 ± 0.01	3/3	0/3	2/2†	2/2†
1	620	47	247	0.66	1/1	0/1	1/1	1/1
4 (Uniform)	620	47	247	0.65	1/1	1/1	1/1	1/1
4 (No AO)	620	47	247	0.63	1/1	1/1	1/1	0/1
1	903	40	210	$0.81 \pm 0.02‡$	0/2	0/2	0/2	0/2
1	903	3	16	0.88‡	0/1	0/1	0/1	0/1
2§	903	88	29	0.83‡	0/7	0/7	0/7	0/7

* Locations were examined for permanent damage in the AOSLO images of the RPE and photoreceptors as well as in color and FA photographs. Table shows the number of times damage was documented for each method/number of trials for each method.

† Although there were three trials for these exposures, only two were examined for permanent damage using photography.

‡ These exposure locations showed full recovery of AF in long-term postexposure images.

§ Experiment 2 illuminated a square retinal area 2° per side.

Images at the same retinal locations 6 days later showed dramatic changes at the photoreceptor and RPE cell levels. For both the 150- and 55- μW cases, disruption of the RPE cell mosaic was observed at the exposure locations. RPE cells were observed in the surrounding areas, but not within the areas exposed to the light (Figs. 1c, 1i). In the 150- μW case, the reflectance image also showed damage in the photoreceptor layer; no photoreceptors were observed at the site of the exposure (Fig. 1f). In the 55- μW case, the photoreceptor layer did not show damage (Fig. 1l) at the exposure location. Table 2 lists how damage was documented for each exposure.

The damage from light exposure was observed 6 days after exposure in the color fundus photograph and the fluorescein angiogram (FA; Fig. 2). Although the exposures were square, the lesions appeared more circular in the color photograph. This is potentially caused by eye motions, which would smooth the edges and corners of the exposure border. The lesions in the FA appeared as window defects and had a donut appearance.

Figure 3 illustrates short-term partial recovery in AF but long-term permanent damage to the RPE and photoreceptors. It shows a series of images from before to 165 days after exposure of the RPE mosaic of a retinal location exposed to 150 μW of 568-nm light for 15 minutes. Immediately after exposure, a decrease in AF was observed at the site of the exposure. However, by 1.5 hours after exposure, this decrease had partially recovered. The AF ratio was 0.66 immediately after exposure compared with 0.76, 1.5 hours after exposure. Damage in the RPE mosaic was observed 11 days after exposure and was still present 165 days after exposure.

Immediate Decrease in AF Intensity after Light Exposure and Long-Term Recovery: Experiments 1 and 2

Figure 4 shows the results from experiment 1 for a retinal location exposed to 40 μW of 568-nm light over 1/2° for 15 minutes. Again, a decrease in AF was observed at the site of the exposure immediately after exposure; the AF ratio was 0.83 immediately after exposure. No change was observed in the photoreceptor image immediately after exposure. No damage was observed at 11 days after exposure in either the reflectance or AF images and the AF ratio had recovered to 0.96.

Figure 5 shows one exposure location from experiment 2 for the pre-, immediately post-, and 8-day postexposure conditions. Across all seven trials, a significant, immediate decrease in AF was observed; the AF ratio immediately after exposure was 0.83 ± 0.01 (mean \pm SE, $t(6) = 14.99$; $P < 0.001$). There was no significant difference between the pre-exposure and the 8-day postexposure AF ratio (0.98 ± 0.02 , mean \pm SE, $t(6) = 1.37$, $P = 0.22$). Figure 6 plots the decrease and recovery of the AF ratio for exposures in experiment 2. No long-term structural changes were observed in the reflectance images or in the RPE AF images (Figs. 5c, 5f). The images shown in Figure 5 are typical of the seven exposures performed in experiment 2.

830-nm Light Exposures: Experiment 3

In experiment 3, we tested the susceptibility of the retina to 1.6 mW for 900 seconds ($8400\text{J}/\text{cm}^2$) of 830-nm light. Figure 7 shows the results of one exposure. No changes in the RPE or photoreceptor layers were observed immediately after exposure or 9 days after exposure. Figure 8 plots the AF ratio before, immediately after, and 6 to 9 days after exposure. Immediately after exposure, the AF ratio was 1.02 ± 0.01 , and 6 to 9 days after exposure the AF ratio was 1.03 ± 0.02 (mean \pm SE). Neither the immediate post- nor the 6- to 9-day postexposure condition is significantly different from the pre-exposure condition where the AF ratio is 1 (immediately postexposure: $t(5) = -2.5$, $P = 0.05$, 6 to 9 days after exposure $t(5) = -1.2$, $P = 0.27$).

Alternative Light-Delivery Methods: Experiment 4

To test whether the retinal damage was caused by AO, scanning, or exposure energy, we delivered light of equivalent average power to the retina with a uniform nonscanning exposure and with the SLO without AO. Figure 9 shows the results of two exposures (150 and 55 μW) delivered with the Maxwellian system. Figure 10 shows the results of two exposures (150 and 55 μW) delivered with the SLO without AO. Immediately after exposure, the AF decreased at the site of the exposure. Figure 11 shows the AF ratio for all three light-delivery methods. There was no significant difference between the magnitudes of AF decrease for the three light-delivery methods (AOSLO versus SLO with AO off: $t(5) = -0.02$, $P = 0.99$, AOSLO versus uniform source: $t(5) = 1.67$, $P = 0.16$, SLO

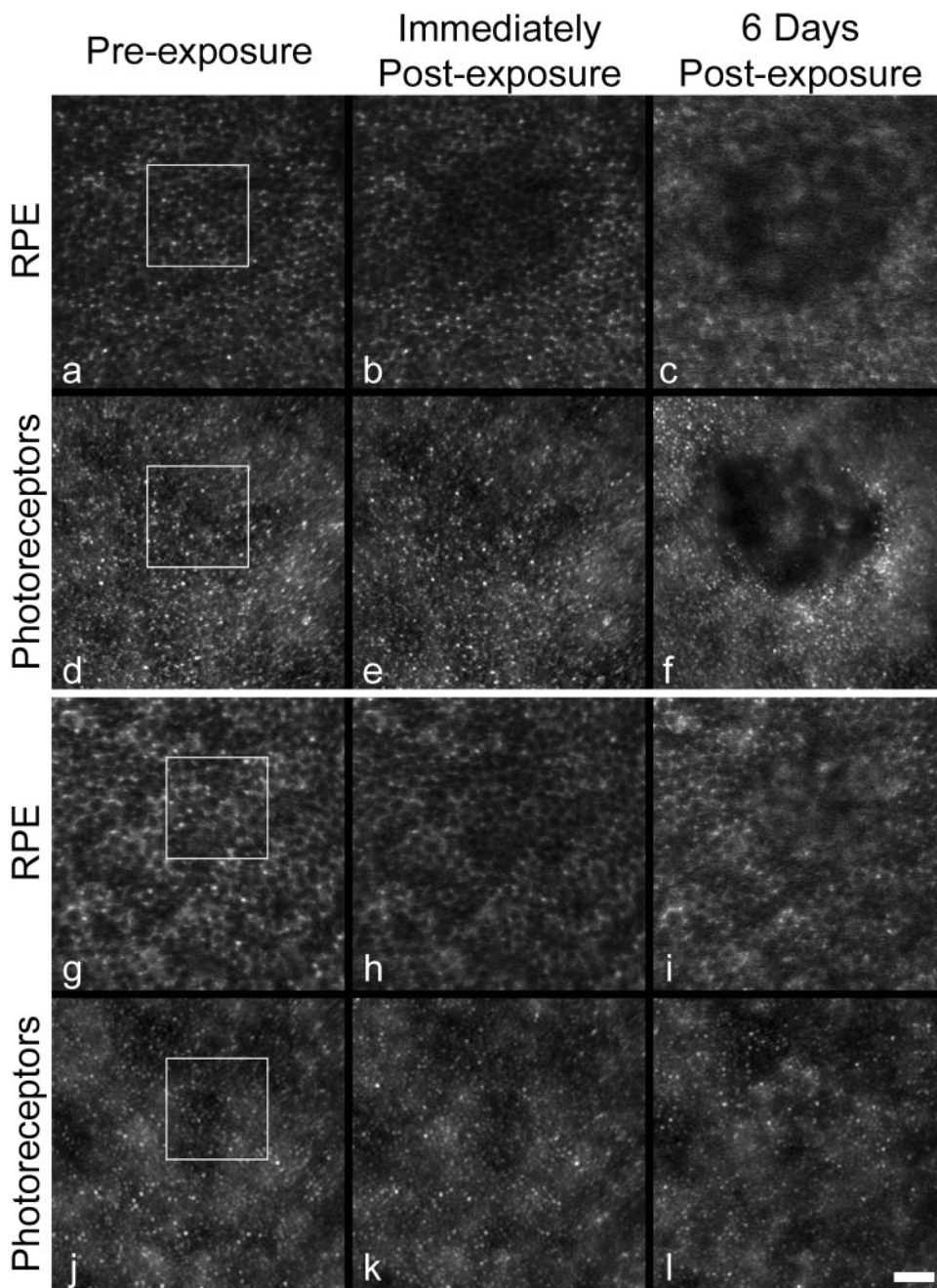


FIGURE 1. Pre-, immediate post-, and 6-day postexposure images of the RPE cells (AF) and the photoreceptor layer (near-infrared reflectance) in locations exposed with the AOSLO to 150 (a-f) or 55 (g-l) μW of 568-nm light for 15 minutes over $1/2^\circ$. *White boxes:* exposure locations. Immediately after exposure, a decrease in AF (b, h) was observed at the site of the exposure. No change was seen in the photoreceptor layer immediately after exposure (e, k). Retinal damage was seen 6 days after 150- μW exposure in the RPE and photoreceptor layer (c, f) and in the RPE cells (i) after 55- μW exposure. No damage was seen in the photoreceptor layer 6 days after 55- μW exposure (j). Scale bar, 50 μm .

with AO off versus uniform source: $t(4) = 1.55$, $P = 0.20$). In all trials, the 55- and the 150- μW exposures caused long-term damage; observations of damage are documented in Table 2. As well, Figure 2 shows the color fundus photograph and FA for these exposures.

DISCUSSION

Alternate Light Delivery of Exposures

Because AOSLO imaging has not been used for light-damage studies, we tested whether the AOSLO light delivery was the cause of the retinal damage. Exposures with alternate methods of delivery (scanning with the SLO without AO or a uniform source) were tested and compared to the AOSLO-delivered exposures of equal average power. For all three light-delivery methods, all exposures with an average power of 47 μW or

more caused permanent retinal damage. Notably, the immediate postexposure decrease in AF intensity was not significantly different between the light-delivery methods (Fig. 11). Thus, the retinal damage was not caused by AO or scanning, but instead was a direct result of the average power delivered to the retina.

Comparison with the Study of Ham et al.

In our study, we detected permanent damage at exposure levels substantially below those reported in the study of Ham et al.,¹ which served as one of the bases for the development of current light-safety standards. They reported threshold lesions for a 1000-second long exposure to be at retinal radiant exposures of 320 J/cm^2 and 4000 J/cm^2 for 514 and 580 nm, respectively (circular exposed area of 1.9° in diameter at the $1/e^2$ points of a Gaussian profile). Wavelength interpolation

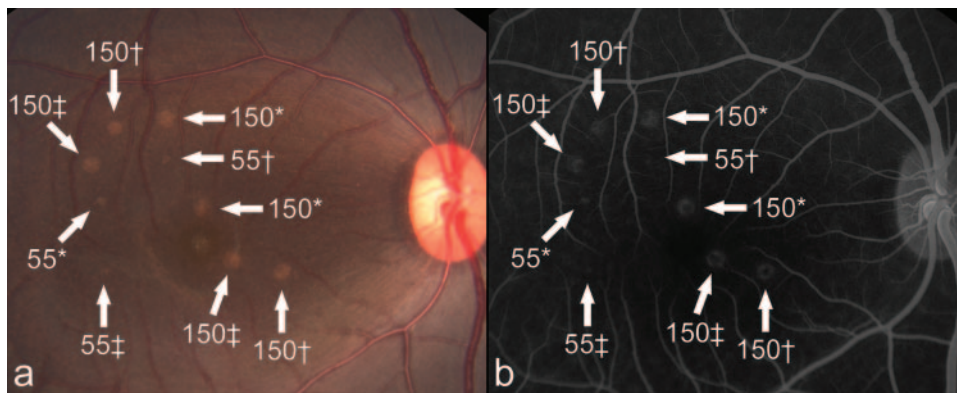


FIGURE 2. Color fundus photograph (a) and fluorescein angiogram (b) 6 days after exposure. The nine exposures showed damage in the color photograph and window defects in the fluorescein angiogram. The number indicated next to each lesion is the power (in μW) of the exposure, followed by one of three symbols: *exposures delivered by the AOSLO (experiment 1), †exposures delivered uniformly without scanning (experiment 4), and ‡exposures delivered by the SLO without AO (experiment 4).

and accounting for the size of the retinal area allows us to estimate that the threshold for 568 nm and a $\frac{1}{2}^\circ$ area would be roughly 3000 J/cm^2 (Fig. 12). In comparison, we observed permanent retinal damage for a 900-second exposure at 568-nm with a power of $47\text{-}\mu\text{W}$ (exposed square area $\frac{1}{2}^\circ$ per side, uniform distribution), or with a retinal radiant exposure of 247 J/cm^2 (assuming a 15-mm focal length). This exposure is an order of magnitude lower than the damage threshold estimated from the data of Ham et al. We did not specifically search for the threshold level by a probit analysis, but given that damage was observed in all trials with 247 J/cm^2 or higher, the 50% damage threshold would be lower than this radiant exposure, thereby further increasing the difference between our results and those of Ham et al.

At 830 nm, thermal threshold damage based on Ham's data occurs at approximately $60,000 \text{ J/cm}^2$, whereas our data showed neither permanent damage nor a postexposure decrease in AF using 8400 J/cm^2 , consistent with the data presented by Ham et al.¹

A potential reason for this discrepancy could be differences in the stability of the retina throughout the long exposure duration. In the present study, the macaque's eye was stabilized, and retinal location was monitored continuously with the AOSLO throughout the 900-second exposure. If the retina moved more than approximately 0.1° in any direction during the exposure, that location was excluded from analysis. Ham et al.¹ do not describe any retinal stability requirements other than anesthesia. Retinal motion could cause substantial differences in lesion threshold values because it reduces the retinal irradiance and consequently increases the threshold levels.

In addition, in the Ham et al.¹ study, the criterion for identifying a lesion was the appearance of a funduscopically visible lesion 48 hours after exposure. In our study, lesion assessment in color fundus images was done 6 days (Fig. 2) or longer after the exposures. The recent emergence of new imaging technologies now allows higher-resolution ophthalmoscopy as an additional endpoint for retinal damage. Here, permanent lesions were detected using AOSLO AF imaging as

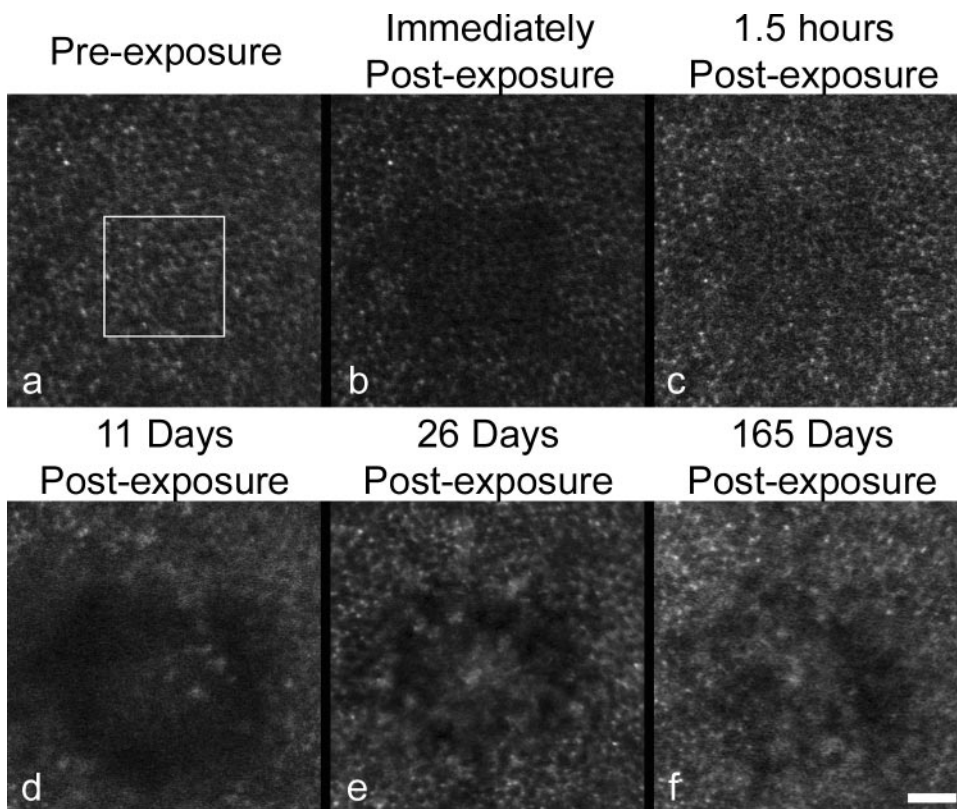


FIGURE 3. Pre-exposure AF image (a) of the RPE cells exposed to $150 \mu\text{W}$ of 568-nm light for 15 minutes over $\frac{1}{2}^\circ$. White boxes: exposure location. Immediately after exposure (b), a decrease in AF was observed at the site of the exposure. At 1.5 hours after exposure (c) the AF had partially recovered, although it was still decreased from the pre-exposure condition. Damage was seen in the RPE cells at the site of the exposure at 11, 26, and 165 days after exposure (d-f, respectively). Adjusting the focus did not bring the RPE mosaic into view at the site of the exposure; therefore, the RPE mosaic was not obscured by retinal edema. Some improvement was observed from 11 days to 26 and 165 days. Scale bar, $50 \mu\text{m}$.

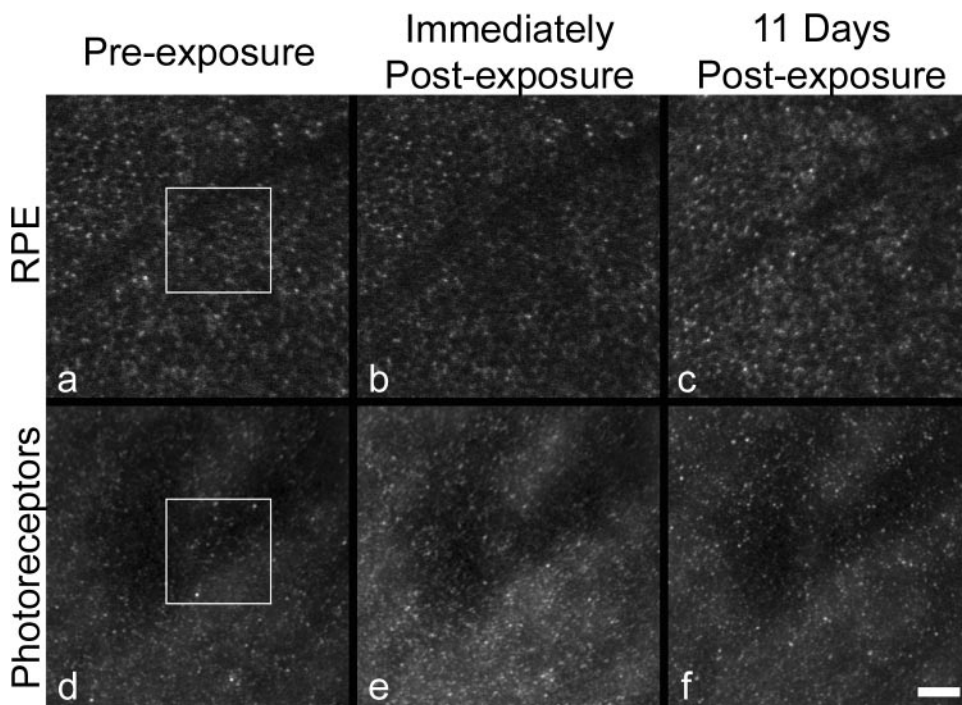


FIGURE 4. Pre-, immediately after, and 11-day postexposure images of the RPE cells and the photoreceptor layer in a location exposed to 40 μ W of 568-nm light for 15 minutes over $\frac{1}{2}^\circ$. *White boxes:* exposure locations. Immediately after exposure (**b**), a decrease in AF was observed at the site of the exposure. RPE AF recovered by 11 days after exposure (**c**). No structural change in the RPE cells was visible between the pre- (**a**), immediate post- (**b**), and 11-day postexposure (**c**) images. In addition, no change was observed in the photoreceptor layer between the pre- (**d**), immediate post- (**e**), and 11-day postexposure (**f**) images. Scale bar, 50 μ m.

the most sensitive measure to date. Although the lesions were confirmed using fundus photography and FA, the lesions (especially the 47- and 55- μ W exposures) were most easily identified by disruption in the RPE cell mosaic observed with the AF AOSLO. That result arises from the ability to image the full RPE mosaic, and thus any structural change in the mosaic is readily observable at the level of a single RPE cell. Future studies to determine the threshold damage level may show that the probit analysis slope is steeper (less variable) over exposure energy when AF RPE AOSLO imaging is used as the metric to determine minimal retinal damage.

Of interest, for our 47 and 55 μ W $\frac{1}{2}^\circ$ exposures (247 and 289 J/cm², respectively), retinal damage in the RPE mosaic was observed with no detectable change in the photoreceptor layer. Thus, the damage appears to originate in the RPE layer. That conclusion is in agreement with several other studies^{2,14,15} of retinal damage, although some studies have shown the initial damage to be in the photoreceptor layer.^{16,45} Because the RPE cells provide support to the photoreceptors, it is believed that cell death in the RPE layer results in subsequent death of the overlying photoreceptors.⁴⁶ Although outside of the scope of the present study, it would be intriguing to observe exposure loca-

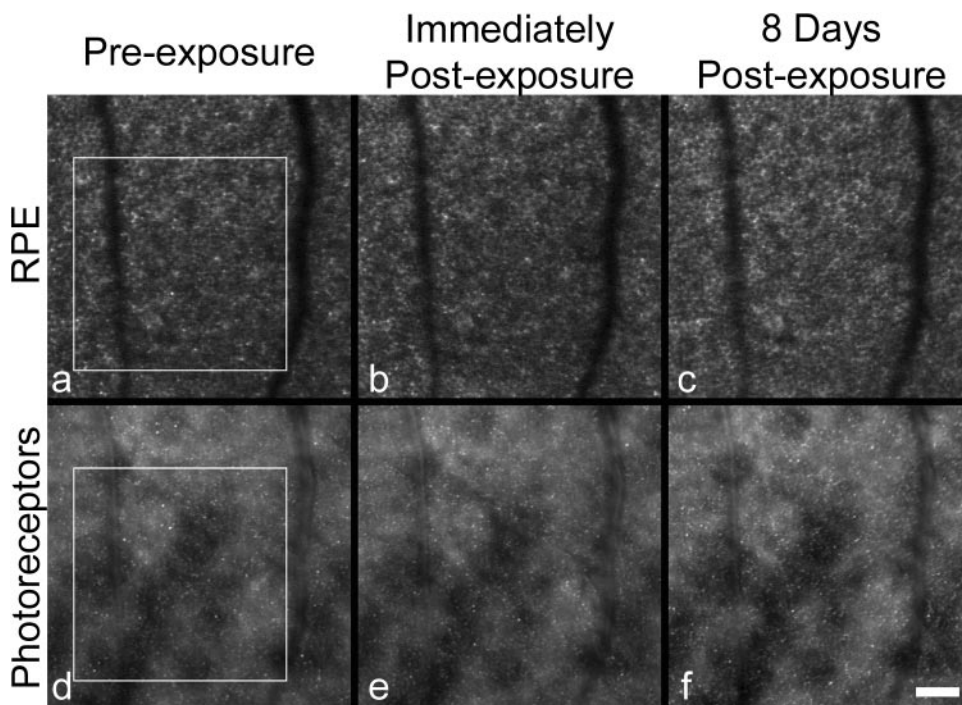


FIGURE 5. Pre-, immediate post-, and 8-day postexposure images of the RPE cells and the photoreceptor layer in a location exposed to 88 μ W of 568-nm light for 15 minutes over 2° . *White boxes:* exposure location. Immediately after exposure (**b**), a decrease in AF was observed at the site of the exposure. RPE AF recovered by 8 days after exposure (**c**). No structural change in the RPE cells was visible between the pre- (**a**), immediate post- (**b**), and 8-day postexposure (**c**) images. In addition, no changes were observed in the photoreceptor layer between the pre- (**d**), immediate post- (**e**), and 8-day postexposure (**f**) images. Scale bar, 100 μ m.

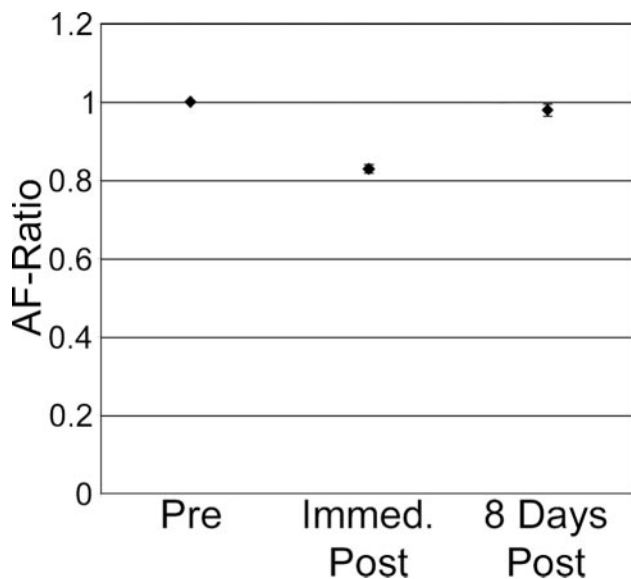


FIGURE 6. AF ratio for 2° exposures of 88 μ W of 568-nm light for 15 minutes. Data points show the mean and SE of the AF ratios from the seven exposures performed in experiment 2.

tions longitudinally that show RPE structural damage but no change in the photoreceptor layer, to determine whether and when the photoreceptor layer begins to degenerate.

Potential Mechanisms for Permanent Damage

Retinal damage for exposure durations longer than approximately 0.1 ms has been shown to occur from thermal mechanisms and/or photochemical mechanisms.^{1,9} For thermal damage to occur, the retinal temperature must increase by approximately 10°C, to result in denaturation of proteins. According to the model presented by Mainster et al.⁴⁷ the 900-second exposures at 568-nm used in this study would cause a maximum increase in retinal temperature of at most 1.5°C.

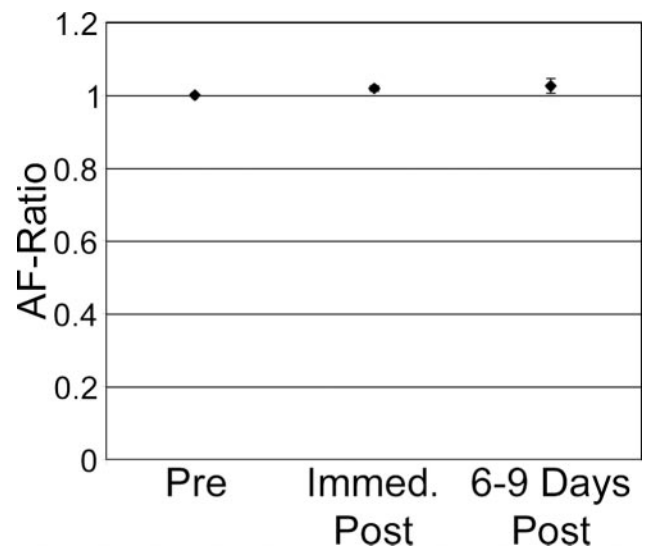


FIGURE 8. AF ratio for 1/2° exposures of 1.6 mW of 830-nm light for 15 minutes. Data points show the mean and SE of the AF ratios from the six exposures performed in experiment 3.

Thus, the damage observed is unlikely to be caused by a thermal mechanism only, but rather by a photochemical or other mechanism. Furthermore, structural damage in the RPE cells was not visible immediately after exposure, but was observed several days after exposure. That observation agrees with other studies,^{1,3} which show that photochemical damage to the retina may not appear until 48 hours after exposure. While the damage in the present study appeared to be the result of a photochemical mechanism, it is interesting to note that the exposure duration was close to the intersection of the two damage mechanisms for this wavelength (Fig. 12). Although photochemical and thermal damage mechanisms are currently treated independently,⁴² we cannot rule out the possibility that the two mechanisms interact such that a small

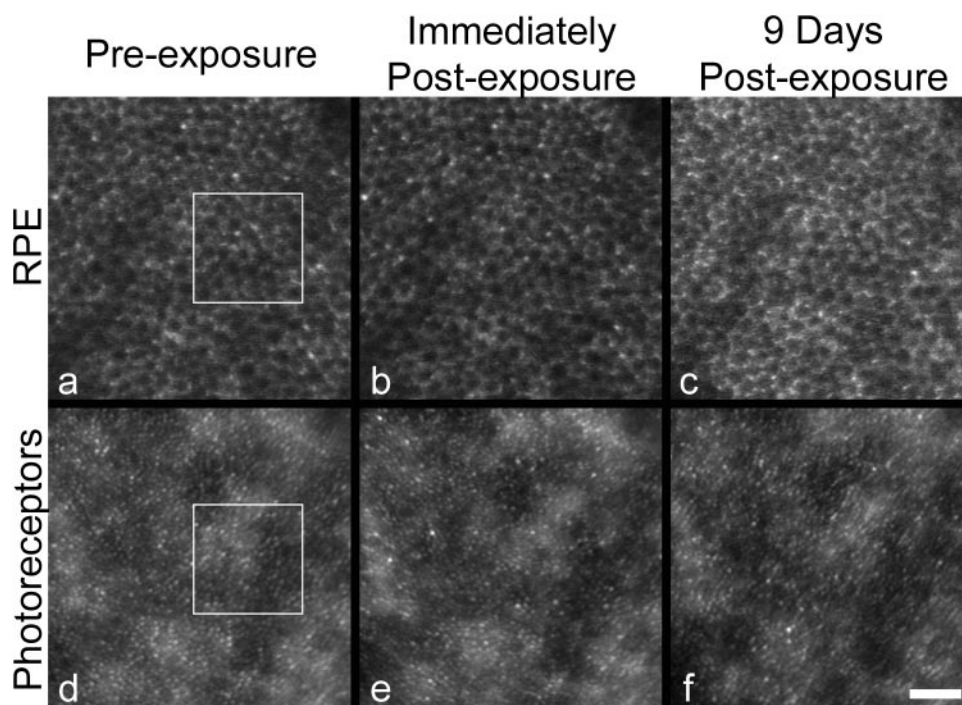


FIGURE 7. Pre-, immediate post-, and 8-day postexposure images of the RPE cells and the photoreceptor layer in a location exposed to 1.6 mW of 830-nm light for 15 minutes over 1/2°. White boxes: exposure location. No changes were observed in the RPE cells or photoreceptor layer between the pre- (a, d), immediate post- (b, e), and 9-day postexposure (c, f) images. Scale bar, 50 μ m.

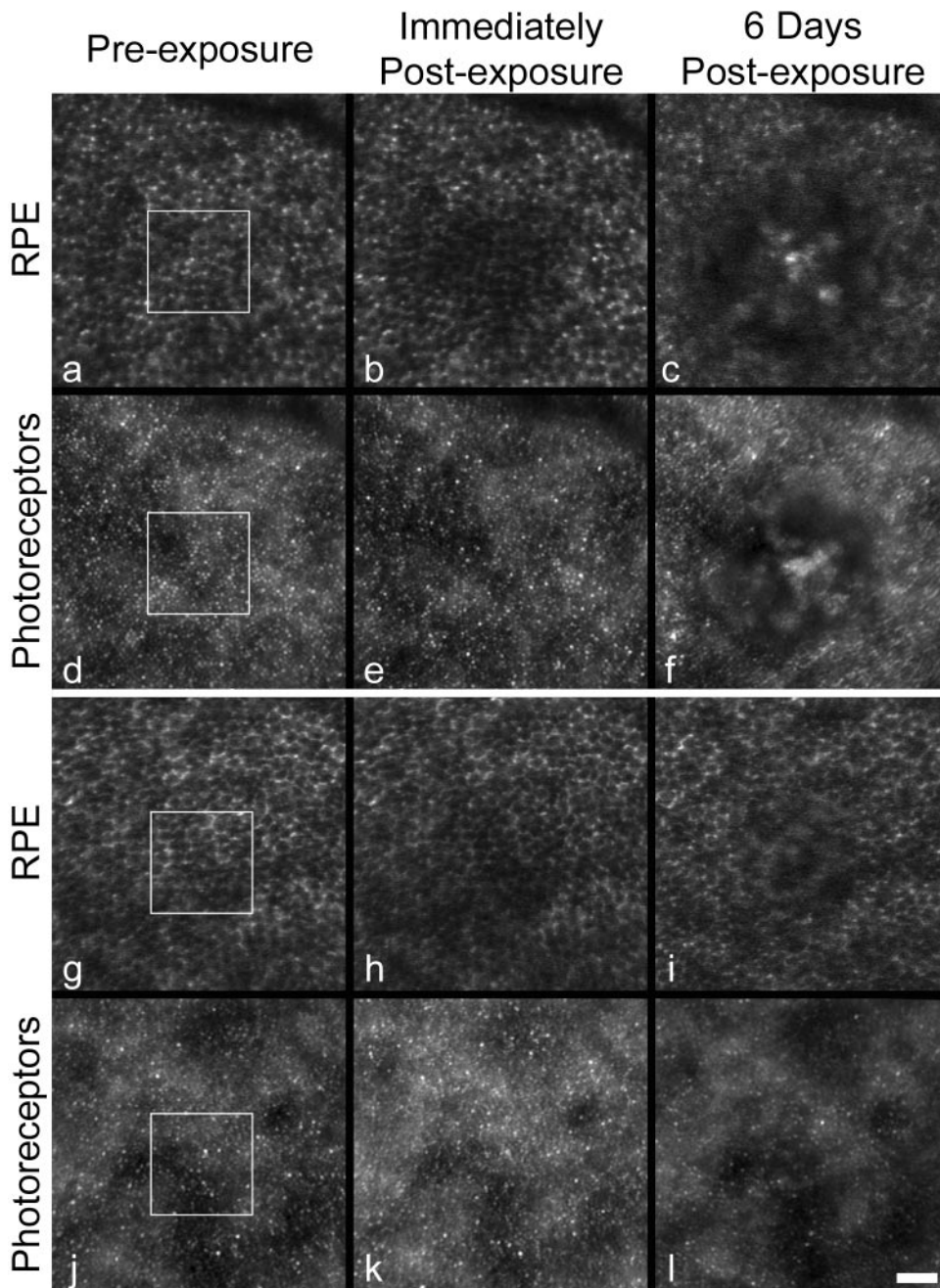


FIGURE 9. Pre-, immediate post-, and 6-day postexposure images of the RPE cells and the photoreceptor layer in locations exposed by a uniform source to 150 (a–f) or 55 (g–l) μW of 568-nm light for 15 minutes over $\frac{1}{2}^\circ$. *White boxes:* exposure location. Immediately after exposure, a decrease in AF (b, h) was observed at the site of the exposure. No change was seen in the photoreceptor layer immediately after exposure (e, k). Retinal damage was seen 6 days after 150- μW exposure in the RPE and photoreceptor layer at 150 μW (c, f) and in the RPE cells (i) at 55 μW . No damage was seen in the photoreceptor layer 6 days after exposure (j) at 55 μW . Scale bar, 50 μm .

rise in temperature would cause a decrease in the photochemical damage threshold. Further work is needed to determine whether these two mechanisms are truly independent.

Photochemical damage may occur by photo-oxidation of lipofuscin.^{48–50} Studies with ARPE-19 (cultured RPE) cells show that the combination of A2E (a constituent of lipofuscin) and blue light (480 nm) cause RPE cell death⁵¹ by a photo-oxidative mechanism.⁴⁹ However, that study⁵¹ also reports significantly less (although some) damage when using green light (545 nm) with radiant exposures of 1260 J/cm², which is approximately 3.7 times higher than the radiant exposures used in the present study. It is notable that ARPE-19 cells, although laden with A2E, do not contain all the pigments contained within RPE lipofuscin. For example, the all-*trans*-retinal dimer series have absorbance maxima at approximately 500 nm and exhibit photoreactivity.²¹ Still other potential

photochemical mechanisms include the absorption of light by the photoreceptors⁹ and the photo-oxidation of RPE melanin,^{52,53} as well as other retinal chromophores.⁹ Thus, although the retinal changes described herein were first observed in the lipofuscin AF signal, it remains to be determined whether lipofuscin photo-oxidation is the cause of the permanent retinal damage.

Potential Mechanisms for the Decrease and Recovery of AF

In addition to permanent retinal damage, we identified a novel retinal change resulting from light exposure: a decrease in the AF at the site of the exposure. Until the mechanism causing the immediate AF decrease and subsequent recovery is better un-

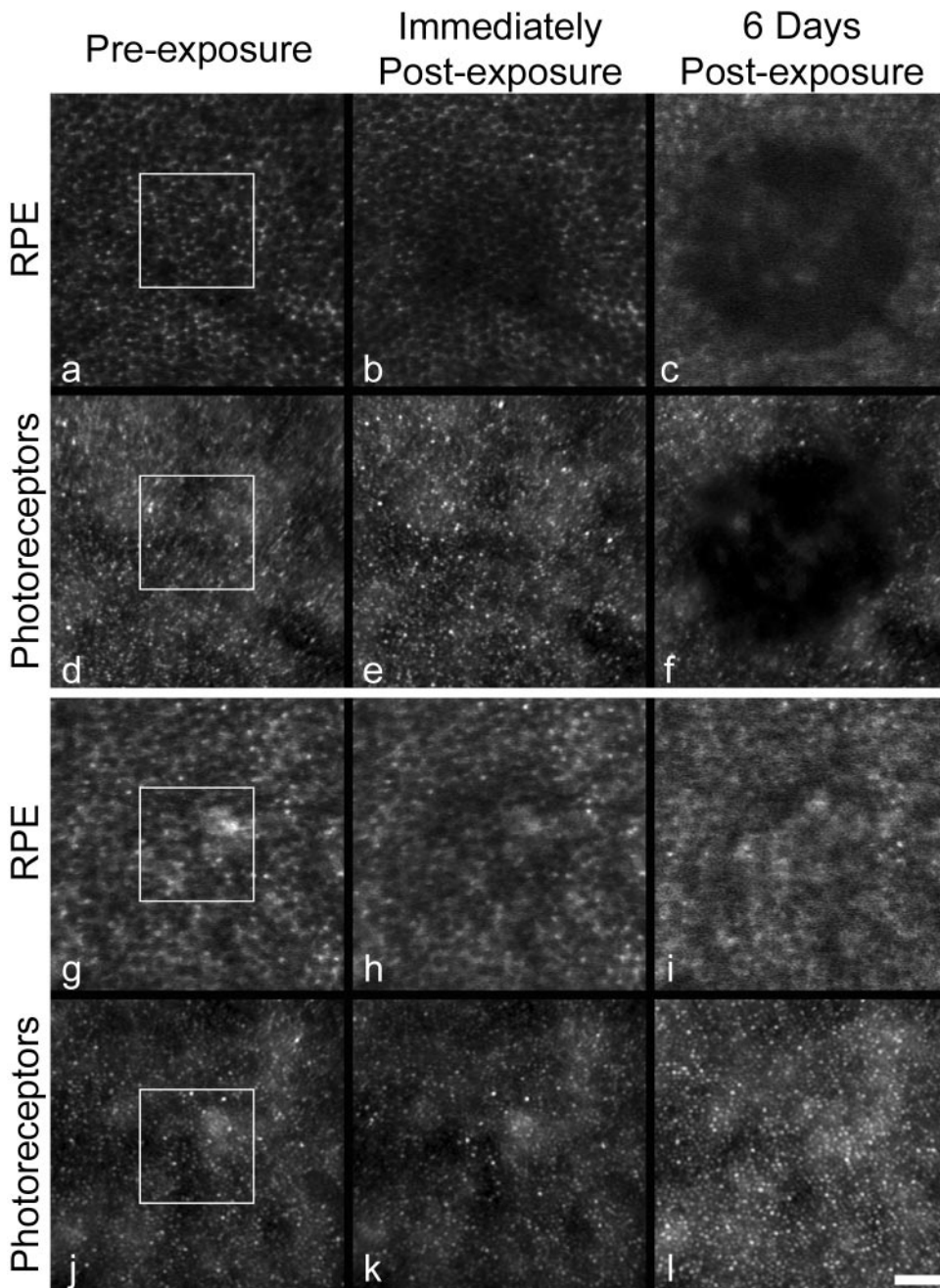


FIGURE 10. Pre-, immediate post-, and 6-day postexposure images of the RPE cells and the photoreceptor layer in locations exposed using the SLO without AO to 150 (a-f) or 55 (g-l) μW of 568-nm light for 15 minutes over $\frac{1}{2}^\circ$. *White boxes:* exposure location. Immediately after exposure, a decrease in AF (b, h) was observed at the site of the exposure. No change was seen in the photoreceptor layer immediately after exposure (e, k). Retinal damage was seen 6 days after exposure in the RPE and photoreceptor layer at the 150- μW exposure (c, f) and in the RPE cells (i) at the 55- μW exposure. No damage was seen in the photoreceptor layer 6 days after exposure (j) at 55 μW . Scale bar, 50 μm .

derstood, it will remain unclear whether this effect is harmful to the retina. The light-induced photo-oxidation of lipofuscin has been shown to cause a decrease in the AF of RPE cells.²⁰ However, our results showed that a decrease in AF can be followed by full recovery of the AF if permanent retinal damage is not observed (Figs. 4, 5, 6). In addition, we showed that partial AF recovery can occur after the initial AF decrease but before permanent retinal damage is observed (Fig. 3c). Although photo-oxidation of lipofuscin may explain the immediate decrease in AF intensity, it currently fails to explain the subsequent recovery. Photoisomerization, in which isomers of lipofuscin molecules are formed, could potentially cause a decrease in AF if the fluorescence spectrum of the isomer is different from that of the original molecule. In addition, the AF recovery could be explained by the isomer's returning to its low-energy state. Further studies are needed to determine

whether photoisomerization and/or photo-oxidation could cause the decrease and recovery of AF described in the present study.

Framme and Roeder⁴⁰ have shown that the AF of lipofuscin can be reversibly decreased by increasing its temperature; they found a linear relationship where a 1°C increase in temperature resulted in a 1% decrease in AF. We present decreases in AF intensity of up to 22% (Table 2) that did not lead to permanent retinal damage. Because a temperature increase of only 10°C is needed to cause a minimal visual lesion and the exposures presented herein are not expected to produce such a temperature increase,⁴⁷ it is unlikely that the 22% decrease in AF is caused by an increase in retinal temperature as described by Framme and Roeder.⁴⁰ Furthermore, such temperature-dependent AF efficiency would result in an immediate recovery after the exposure that is not observed in the present study.

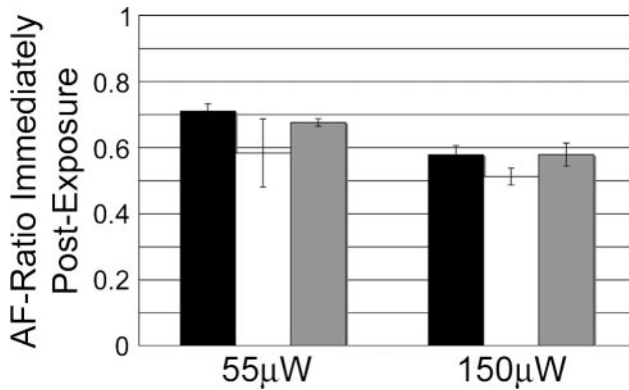


FIGURE 11. AF ratios immediately after exposure for the three exposure delivery methods: AOSLO with AO (■), uniform source (□), and SLO without AO (▣). Error bars, SE. There was no significant difference in the AF decrease between light-delivery methods. However, the 150- μ W exposures had a significantly greater effect than did the 55- μ W exposures.

Another potential mechanism is fluorescence recovery after photobleaching (FRAP), which has been used to estimate diffusion constants of molecules.⁵⁴ However, the recovery of the photobleached area in FRAP studies occurs within seconds⁵⁵—substantially faster than the recovery observed in our study.

Although lipofuscin accumulates naturally in RPE cells over time, the recovery in AF is not due to the normal formation of additional molecules over the time described in this study. Over a period of 30 years, the AF doubles in humans²³; therefore, in a period of 6 days, the lipofuscin would increase by only 1.0005 by the normal lipofuscin formation mechanisms, which is certainly not enough to explain the recovery observed in this study (Fig. 6).

The observed decrease in AF and its recovery could also be the result of changes outside of the lipofuscin granules. For instance, transient changes in the RPE melanin or overlying photoreceptors could result in blocked or decreased efficiency in lipofuscin AF. In addition, spectral changes in lipofuscin AF (for example those observed by Parish et al.⁵⁶ in synthesized A2E) could result in decreased AF, especially given that 568-nm light is located halfway down the lipofuscin excitation spectrum on the long-wavelength side.¹⁹

Thus, the mechanism for the decreased AF after light exposure remains largely unexplained. In results to be presented elsewhere, we have observed a decrease in AF followed by partial recovery of AF in fixed donor RPE cells and fixed cultured RPE cells. Further *ex vivo* studies of extracted lipofuscin and RPE preparations may help determine to what extent nonbiological mechanisms (such as changes in the fluorescence efficiency or the fluorescence spectrum) are responsible for these observations. It is important to learn the mechanism behind the AF decrease to determine the safety of light exposures causing these changes.

Exposures Compared to the ANSI Standard

Light safety standards, including the ANSI Standard⁵ were developed to protect healthy and alert individuals in occupational settings from hazardous exposures to lasers and other sources. Underlying assumptions in the Standard are that the exposure overfills the pupil, that the pupil constricts for visible radiation for $t > 1$ second (light reflex), and that eye and head movements spread the light of small sources on the retina thereby reducing the hazard potential for long exposure durations (longer than $t_2 = 10$ to 100 seconds for the thermal limits, and longer than 100 to 10^4 seconds for the photochemical limits).

With ophthalmic instruments, however, the pupil is often dilated by drugs, Maxwellian illumination may be used, and eye and head movements are minimized by the use of a chin/head rest and a fixation target. The Standard addresses the situation of ophthalmic applications (§8.3), recommending in essence that these assumptions be ignored: The limiting levels must be reduced for $\lambda < 600$ nm and $t > 0.07$ seconds when the pupil is dilated and also for long exposure durations when eye/head movements are restricted. Delori et al.⁴² recently “translated”

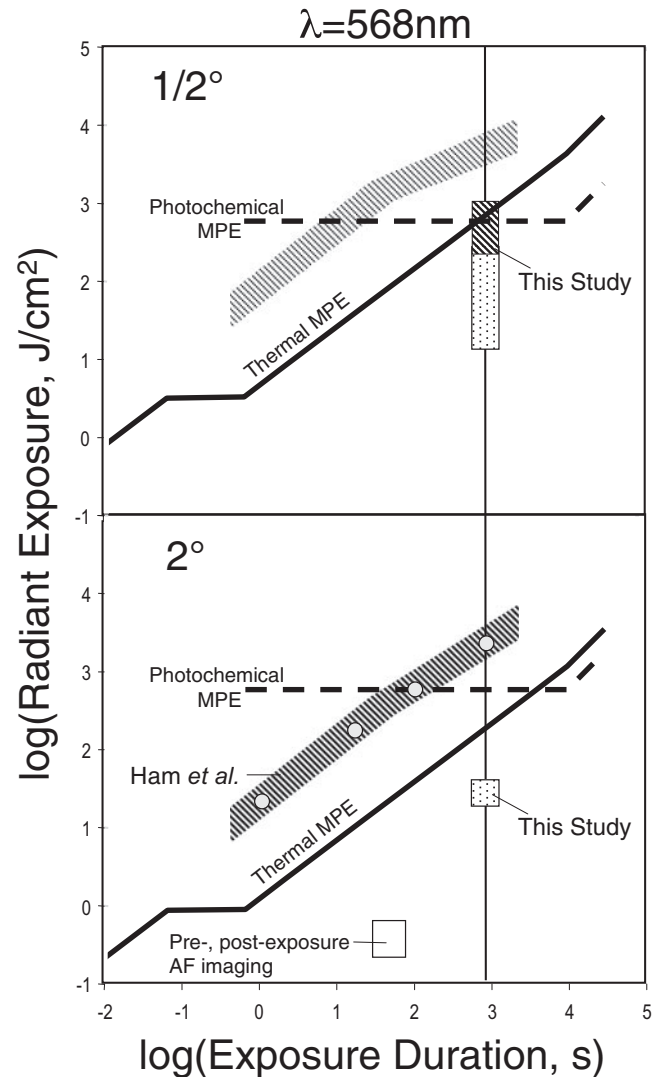


FIGURE 12. Plot of radiant exposure (joules per square centimeter) at 568-nm versus exposure duration (seconds) for an exposed area of $1/2^\circ$ (top) and of 2° (bottom). *Cross-hatched areas (bottom)*: exposure conditions at which Ham et al.¹ reported threshold damage (interpolated between their 515- and 580-nm data). This damage was assessed as being a combination of thermal damage (short durations) and photochemical damage (long durations); (top) estimation of threshold damage for a $1/2^\circ$ exposed area (accounting for the change in size of the exposed area). Thus, threshold damage at 900 seconds would be at approximately 3000 J/cm^2 , or nearly 10 times higher than the radiant exposures at which we observed permanent damage (*cross-hatched rectangles*). *Dotted rectangles*: radiant exposures at which we observed decreased AF with full recovery; *white square*: radiant exposures used for pre- and postexposure imaging. The variations of MPE versus time for thermal (*solid line*) and photochemical (*dashed line*) are also shown in both plots. Note that the photochemical limit was independent of the size of the exposed area, whereas the thermal limit decreased (by a factor of 4) with increased size.

the ANSI Standard into a form that is both more practical and directly applicable for ophthalmic application. The study explained some of the intricacies of the Standard and incorporated the removal of these assumptions. It also addressed the light exposure safety for the SLO (see the Appendix).⁴²

The ANSI standard sets MPE limits depending on the exposure wavelength, exposure duration, and size of the exposed area on the retina. These MPEs were selected on the basis of experimental determinations of threshold levels for retinal damage. Damage threshold is defined as the level at which examiners would detect minimal damage 50% of the time (ED-50).⁵⁷ The MPE level is then set at approximately one order of magnitude below the damage threshold; this provides exposure levels with minimal risk for damage in humans from exposure.⁵⁷ The thermal and photochemical ANSI MPE limits for 568-nm are given in Figure 12 for exposures over $\frac{1}{2}^\circ$ and 2° .

The MPE for the macaque retina (adjusted from the human retina MPE by using a focal length of 15 mm) for a 15-minute exposure of 568 nm over $\frac{1}{2}^\circ$ is $107 \mu\text{W}$ (photochemical limit, see the Appendix and Fig. 12).^{5,42} We observe permanent retinal damage by both AOSLO imaging and by color photography at exposures equal or higher than $47 \mu\text{W}$ (Table 2), and thus at levels that are nearly 2.3 times lower than the permissible exposure where no damage should be observed (Fig. 12). The monkey eye is believed to be more susceptible to retinal damage than the human because of the higher RPE melanin pigment density.⁵⁷ If thermal and photochemical mechanisms are not independent but instead interact with each other, then the higher RPE melanin pigment density could effect both the thermal and photochemical thresholds.

The MPE for the macaque retina for a 15-minute exposure of 830 nm over $\frac{1}{2}^\circ$ is $627 \mu\text{W}$ (thermal limit, see Appendix). Our 1.6-mW exposures at 830-nm are 2.55 times above this MPE level. The exposures neither resulted in permanent retinal damage nor in a decrease in AF. Thus, our results for the 830-nm exposures are consistent with the ANSI Standard since damage would be expected only at levels approximately 10 times higher than the MPE. Higher-powered exposures were not tested because 1.6 mW was the highest power that could be delivered through the AOSLO with our current laser diode.

Exposures in this study consisted of three wavelengths simultaneously illuminating the retina. Although few studies have tested the safety of multiple wavelength laser exposures,⁵⁸ the ANSI Standard does provide guidelines for simultaneous exposures to multiple wavelengths as proposed by Lyon⁵⁹ (detailed in the Appendix). When accounting for the multiple wavelengths, the MPE is reduced by a factor of 1.4 (reduced from 107 to $75 \mu\text{W}$, see Appendix) for the 568-nm, 900-second exposures. Therefore, all exposures below $75 \mu\text{W}$ of 568-nm are still below the ANSI MPE. Accounting for multiple wavelengths does not resolve the discrepancy between the damage levels observed in this study and the current ANSI Standard.

Pre- and postexposure images were acquired over a 2° square area for 60 seconds with exposure to all three wavelengths. Accounting for all three wavelengths, the light levels used for 568-nm were 19 times below the ANSI MPE for these image exposures. However, test exposures of $3 \mu\text{W}$ for 900 seconds of 568 nm over $\frac{1}{2}^\circ$ (25 times lower than the ANSI standard MPE) caused a decrease in AF. Therefore, the pre- and postexposure images may have caused a decrease in AF over the entire field imaged. No long-term damage was found from routine imaging at any location. To optimize routine imaging conditions, future studies will be necessary to determine the threshold for the decrease in AF.

CONCLUSIONS

This study shows that fluorescence AOSLO imaging provides high-resolution AF images of the RPE as well as a sensitive method to assess RPE damage including that caused by light exposure.

Permanent structural damage in the RPE mosaic was observed in this study after exposures between 47 and $150 \mu\text{W}$ of 568 nm for 900 seconds over $\frac{1}{2}^\circ$. The damage was documented by AOSLO AF imaging, 830-nm reflectance imaging, color imaging, and FA.

Expressed as a percentage of the MPE, these exposures were 50% to 200% of the MPE given by the ANSI Standard. Because the MPE is generally a factor of 10 below the retinal damage threshold, none of our exposures should have resulted in the observed damage.

Thus, the ANSI Standard and other safety guidelines appear to provide insufficient protection for the long exposures over the small retinal area used in this study. Such exposures have been investigated in only a few studies,¹ perhaps because they are not applicable to alert individuals in occupational settings. Nevertheless, the safety limits should reflect biological data and we hope that—as in the past as a result of new data—the ANSI Standard and other safety guidelines will introduce the appropriate revisions to provide adequate safety.

These findings are particularly important because some clinical procedures (such as slit lamp examination, fundus photography, FA, and retinal surgery) are often performed at light levels close to the MPE.^{60–62} The higher sensitivity of a modern clinical SLO, however, allows FA and autofluorescence imaging to be performed at levels that are less than one tenth of the MPE.⁴² It should also be stressed that clinical instruments are typically used on patients with retinal diseases or other retinal abnormalities. It has been shown that certain genetic mutations can cause higher susceptibility to light in animal models,⁶³ and it remains unknown the extent to which patients with retinal diseases have increased susceptibility to retinal light damage.

In addition, this study describes a novel retinal change, a decrease in the AF intensity as a result of light exposure to the retina. This decrease in AF was observed even at the lowest exposure power tested, $3 \mu\text{W}$ for 900 seconds of 568 nm over $\frac{1}{2}^\circ$ (25 times lower than the ANSI MPE). Therefore, future studies are necessary to determine the threshold levels of light that cause a decrease in AF, the action spectrum of the phenomenon, and whether this effect is detrimental to retinal health.

Acknowledgments

The authors thank Richard Wang, Drew Scoles, William Fischer, Jens Buehren, Janet R. Sparrow, and Edward N. Pugh, Jr. for assistance.

References

1. Ham WTJ, Mueller HA, Ruffolo JJ, Clarke AM. Sensitivity of the retina to radiation damage as a function of wavelength. *Photochemistry and Photobiology*. 1979;29:735–743.
2. Ham WTJ, Ruffolo JJJ, Mueller HA, et al. Histologic analysis of photochemical lesions produced in rhesus retina by short-wavelength light. *Invest Ophthalmol Vis Sci*. 1978;17(10):1029–1035.
3. Lund DJ, Stuck BE, Edsall P. Retinal injury thresholds for blue wavelength lasers. *Health Physics*. 2006;90(5):477–484.
4. Schuele G, Rumohr M, Huettmann G, Brinkmann R. RPE damage thresholds and mechanisms for laser exposure in the microsecond-to-millisecond time regimen. *Invest Ophthalmol Vis Sci*. 2005;46:714–719.
5. ANSI. American National Standard for Safe Use of Lasers ANSI Z136.1-2007: Laser Institute of America, 2007.

6. ACGIH. American Conference of Governmental Industrial Hygienists; TLVs and BEIs. ACGIH. Cincinnati, OH; 2005.
7. ICNIRP. International Commission on Non-Ionizing Radiation Protection: Guidelines on limits of exposure to laser radiation of wavelengths between 180nm and 1,000 microns. *Health Physics* 1996;71:804-819.
8. ICNIRP. Revision of guidelines on limits of exposure to laser radiation of wavelengths between 400 nm and 1.4 micron. International Commission on Non-Ionizing Radiation Protection. *Health Physics*. 2000;79(4):431-440.
9. Glickman RD. Phototoxicity to the retina: mechanisms of damage. *Int J Toxicol*. 2002;21(6):473-490.
10. Lund DJ. Action spectrum for retinal thermal injury. In: Matthes R, Sliney DH, eds. *Measurements of Optical Radiation Hazards*. Munich: Maerkl-Druck; 1998:209-228.
11. Stuck BE. The Retinal and Action Spectrum for Photoretinitis ("Blue-Light Hazard"). In: Matthes R, Sliney DH, eds. *Measurements of Optical Radiation Hazards*. Munich: Maerkl-Druck; 1998:193-208.
12. Clarke AM, Geeraets WJ, Ham WTJ. An equilibrium thermal model for retinal injury from optical sources. *Appl Opt*. 1969;8(5):1051-1054.
13. Dawson W, Nakanishi-Ueda T, Armstrong D, et al. Local fundus response to blue (LED and laser) and infrared (LED and laser) sources. *Exp Eye Res*. 2001;73:137-147.
14. Masuda K, Watanabe I. Short wavelength light-induced retinal damage in rats. *Jpn J Ophthalmol*. 2000;44:615-619.
15. Kawano T, Kato M. Electrophysiologic evaluation of retinal pigment epithelial damage induced by photopic exposure. *Retina*. 2003;23:513-517.
16. Adams DO, Beatrice ES, Bedell RB. Retina: ultrastructural alterations produced by extremely low levels of coherent radiation. *Science*. 1972;177:58-60.
17. von Ruckmann A, Fitzke FW, Bird AC. Distribution of fundus autofluorescence with a scanning laser ophthalmoscope. *Br J Ophthalmol*. 1995;79:407-412.
18. von Ruckmann A, Fitzke FW, Bird AC. Fundus autofluorescence in age-related macular disease imaged with a laser scanning ophthalmoscope. *Invest Ophthalmol Vis Sci*. 1997;38:478-486.
19. Delori FC, Dorey CK, Staurengi G, et al. In vivo fluorescence of the ocular fundus exhibits retinal pigment epithelium lipofuscin characteristics. *Invest Ophthalmol Vis Sci*. 1995;36(3):718-729.
20. Sparrow JR, Boulton M. RPE lipofuscin and its role in retinal pathobiology. *Exp Eye Res*. 2005;80:595-606.
21. Fishkin NE, Sparrow JR, Allikmets R, Nakanishi K. Isolation and characterization of a retinal pigment epithelial cell fluorophore: an all-trans-retinal dimer conjugate. *Proc Natl Acad Sci USA*. 2005; 102(20):7091-7096.
22. Delori FC. Spectrophotometer for noninvasive measurement of intrinsic fluorescence and reflectance of the ocular fundus. *Applied Optics*. 1994;33(31):7439-7452.
23. Delori FC, Goger DG, Dorey CK. Age-related accumulation and spatial distribution of lipofuscin in RPE of normal subjects. *Invest Ophthalmol Vis Sci*. 2001;42(8):1855-1866.
24. Bindewald A, Jorzik JJ, Loesch A, et al. Visualization of retinal pigment epithelial cells in vivo using digital high-resolution confocal scanning laser ophthalmology. *Am Ophthalmol*. 2004; 137(3):556-558.
25. Liang J, Williams DR, Miller DT. Supernormal vision and high-resolution retinal imaging through adaptive optics. *J Opt Soc Am A*. 1997;14(11):2884-2892.
26. Hofer H, Chen L, Yoon GY, et al. Improvement in retinal image quality with dynamic correction of the eye's aberrations. *Opt Express*. 2001;8(11):631-643.
27. Roorda A, Romero-Borja F, Donnelly III WJ, et al. Adaptive optics scanning laser ophthalmology. *Opt Express*. 2002;10(9):405-412.
28. Gray DC, Merigan W, Wolfing JI, et al. In vivo fluorescence imaging of primate retinal ganglion cells and retinal pigment epithelial cells. *Opt Express*. 2006;14:7144-7158.
29. Hermann B, Fernandez EJ, Unterhuber A, et al. Adaptive-optics ultrahigh-resolution optical coherence tomography. *Opt Lett*. 2004;29(18):2142-2144.
30. Zawadzki RJ, Choi SS, Jones SM, et al. Adaptive optics-optical coherence tomography: optimizing visualization of microscopic retinal structures in three dimensions. *J Opt Soc Am A*. 2007;24(5): 1373-1383.
31. Merino D, Dainty C, Bradu A, Podoleanu AG. Adaptive optics enhanced simultaneous en-face optical coherence tomography and scanning laser ophthalmology. *Opt Express*. 2006;14(8): 3345-3353.
32. Roorda A, Williams DR. The arrangement of the three cone classes in the living human eye. *Nature (Lond)*. 1999;397:520-522.
33. Pallikaris A, Williams DR, Hofer H. The reflectance of single cones in the living human eye. *Invest Ophthalmol Vis Sci*. 2003;44(10): 4580-4592.
34. Carroll J, Neitz M, Hofer H, et al. Functional photoreceptor loss revealed with adaptive optics: an alternate cause for color blindness. *Proc Natl Acad Sci USA*. 2004;101(22):8461-8466.
35. Wolfing JI, Chung M, Carroll J, et al. High-resolution retinal imaging of cone-rod dystrophy. *Ophthalmology*. 2006;113:1014-1019.
36. Roorda A, Zhang Y, Duncan JL. High-resolution in vivo imaging of the RPE mosaic in eyes with retinal disease. *Invest Ophthalmol Vis Sci*. 2007;48(5):2297-2303.
37. Martin JA, Roorda A. Direct and noninvasive assessment of parafoveal capillary leukocyte velocity. *Ophthalmology*. 2005;112:2219-2224.
38. Vilupuru AS, Rangaswamy NV, Frishman IJ, et al. Adaptive optics scanning laser ophthalmology for in vivo imaging of lamina cribrosa. *J Opt Soc Am A*. 2007;24(5):1417-1425.
39. Framme C, Brinkmann R, Birngruber R, Roeder J. Autofluorescence imaging after selective RPE laser treatment in macular diseases and clinical outcome: a pilot study. *Br J Ophthalmol*. 2002;86:1099-1106.
40. Framme C, Schüle G, Roeder J, Birngruber R, Brinkmann R. Online autofluorescence measurements during selective RPE laser treatment. *Graefes Arch Clin Exp Ophthalmol*. 2004;2004(242):863-869.
41. Framme C, Roeder J. Immediate and long-term changes of fundus autofluorescence in continuous wave laser lesions of the retina. *Ophthalmic Surg Lasers Imag*. 2004;35:131-138.
42. Delori FC, Webb RH, Sliney DH. Maximum permissible exposures for ocular safety (ANSI 2000), with emphasis on ophthalmic devices. *J Opt Soc Am A*. 2007;24(5):1250-1265.
43. Metha AB, Crane AM, Rylander HGI, et al. Maintaining the cornea and the general physiological environment in visual neurophysiology experiments. *J Neurosci Methods*. 2001;109:153-166.
44. Wyszecki G, Stiles WS. *Color Science: Concepts and Methods, Quantitative Data and Formulae*. 2nd ed. New York: John Wiley & Sons; 1982:98-101.
45. Sykes SM, Robison WGJ, Waxler M, Kuwabara T. Damage to the monkey retina by broad-spectrum fluorescent light. *Invest Ophthalmol Vis Sci*. 1981;20(4):425-434.
46. Strauss O. The retinal pigment epithelium in visual function. *Physiol Rev*. 2005;85(3):845-881.
47. Mainster MA, White TJ, Tips JH, Wilson PW. Retinal-temperature increases produced by intense light sources. *J Opt Soc Am*. 1970; 60(12):264-270.
48. Davies S, Elliott MH, Floor E, et al. Phototoxicity of lipofuscin in human retinal pigment epithelial cells. *Free Radic Biol Med*. 2001; 31(2):256-265.
49. Sparrow JR, Zhou J, Ben-Shabat S, et al. Involvement of oxidative mechanisms in blue-light-induced damage to A2E-laden RPE. *Invest Ophthalmol Vis Sci*. 2002;43:1222-1227.
50. Lamb LE, Simon JD. A2E: a component of ocular lipofuscin. *Photochem Photobiol*. 2004;79(2):127-136.
51. Sparrow JR, Nakanishi K, Parish CA. The lipofuscin fluorophore A2E mediates blue light-induced damage to retinal pigmented epithelial cells. *Invest Ophthalmol Vis Sci*. 2000;41:1981-1989.
52. Sarna T, Burke JM, Korytowski JM, et al. Loss of melanin from human RPE with again: possible role of melanin photooxidation. *Exp Eye Res*. 2003;76:89-98.
53. Burke JM, Henry MM, Zareba M, Sarna T. Photobleaching of melanosomes from retinal pigment epithelium: 1. Effects on protein oxidation. *Photochem Photobiol*. 2007;83:920-924.

54. Lopez A, Dupou L, Altibelli A, Trotard J. Fluorescence recovery after photobleaching (FRAP) experiments under conditions of uniform disk illumination: critical comparison of analytical solutions, and a new mathematical method for calculation of diffusion coefficient D. *Biophys J*. 1988;53:963-970.
55. Pucadyil TJ, Chattopadhyay A. Confocal fluorescence recovery after photobleaching of green fluorescent protein in solution. *J Fluorescence*. 2006;16(1):87-94.
56. Parish CA, Hashimoto M, Nakanishi K, et al. Isolation and one-step preparation of A2E and iso-A2E, fluorophores from human retinal pigment epithelium. *Proc Natl Acad Sci USA*. 1998;95:14609-14613.
57. Sliney DH, Mellerio J, Gabel VP, Schulmeister K. What is the meaning of threshold in laser injury experiments? Implications for human exposure limits. *Health Physics*. 2002;82(3):335-347.
58. Roach W, Thomas R, Buffington G, et al. Simultaneous exposure using 532 and 860 nm lasers for visible lesion thresholds in the rhesus retina. *Health Physics*. 2006;90(3):241-249.
59. Lyon TL. Hazard analysis technique for multiple wavelength lasers. *Health Physics*. 1985;49:221-226.
60. Delori FC, Parker JS, Mainster MA. Light levels in fundus photography and fluorescein angiography. *Vision Res*. 1980;20:1099-1104.
61. Delori FC, Pomerantzeff O, Mainster MA. Light levels in ophthalmic diagnostic instruments. *Soc Photo-Opt Instrument Eng*. 1980; 229:154-160.
62. Stiller H, Rassow B. Light hazards to the patient's retina from ophthalmic instruments. *Appl Opt*. 1991;30(16):2187-2196.
63. Cideciyan AV, Jacobson SG, Aleman TS, et al. In vivo dynamics of retinal injury and repair in the rhodopsin mutant dog model of human retinitis pigmentosa. *Proc Natl Acad Sci USA*. 2005; 102(14):5233-5238.

APPENDIX

ANSI Maximum Permissible Exposures

The ANSI Standard⁵ expresses its MPEs as radiant exposure at the cornea as a function of wavelength (λ), exposure duration (t), and angular size of the exposed area (α). The ANSI Standard does not explicitly cover the complex light exposure of an SLO, and simulations of the exposures are therefore introduced to assess the hazard potential.

One simulation is that of a continuous beam uniformly distributed over the entire field.⁴² For *thermal damage*, the maximum permissible radiant power through the pupil (in watts), for $400 \text{ nm} < \lambda < 1050 \text{ nm}$ and for $18 \mu\text{s} < t < 10^4$ seconds, can be equated as:

$$MPE_{\text{thermal}} = \{1.8 \times 10^{-3} C_A C_E T^{0.75}\} \left(\frac{A_{p,7}}{P} \frac{1}{T} \right) \quad (A1)$$

$$= 6.93 \times 10^{-4} \frac{C_A C_E}{P T^{0.25}},$$

where the term in curly brackets is the ANSI limiting radiant exposure at the cornea (J/cm^2 ; ANSI Table 5b⁵), and the term in parentheses converts the limiting corneal radiant exposure into the limiting radiant power through the pupil. The different parameters are:

C_A = a wavelength-dependent ANSI parameter that is a crude representation of the absorption by melanin; $C_A = 1$ for $\lambda < 700 \text{ nm}$, and $C_A = 10^{0.002(\lambda - 700)}$ for $700 < \lambda < 1050 \text{ nm}$ (1.00 for 568 nm, 1.82 for 830 nm, and 2.56 for 904 nm).

C_E = the scaling factor for extended sources. For a square field $C_E = 4\alpha/(4\pi\alpha_{\text{min}})$ where α is the angle (in millirads) subtending the side of the field ($\alpha = 8.73 \text{ mrad}$ for $1/2^\circ$, $\alpha_{\text{min}} = 1.5 \text{ mrad}$, and $C_E = 7.41$).

TABLE A1. Maximum Permissible Average Power at the Pupil ($t = 900 \text{ s}$)

Wavelength	Thermal (Eq. 1)	Photochemical (Eq. 2)	SLO (Eq. 4)
Exposure Size $1/2^\circ \times 1/2^\circ$			
$\lambda = 568$	134 μW	107 μW	345 μW^* , 152 μW^\dagger
$\lambda = 830$	1.33 mW	—	627 μW
$\lambda = 904$	1.87 mW	—	883 μW
Exposure Size $2^\circ \times 2^\circ$			
$\lambda = 568$	538 μW	1.71 mW	604 μW^* , 266 μW^\dagger
$\lambda = 830$	5.32 mW	—	1.10 mW
$\lambda = 904$	7.49 mW	—	1.55 mW

Bold numbers show the limiting simulation for the MPE.

* SLO simulation with no blanking; ON ratio = 1.

† SLO simulation with blanking; ON ratio = 0.37.

$A_{p,7}$ = the area of a 7-mm-diameter pupil (0.385 cm^2).

P = dimensionless factor that accounts for the removal of the assumption about the pupil diameter (ANSI 8.3).

For exposure duration longer than 0.7 seconds, $P = 1$ for $\lambda > 700 \text{ nm}$, and $P = 5.44$ for $\lambda < 600 \text{ nm}$.

t = the exposure duration (in seconds).

The thermal limits are calculated by substitution of all relevant parameters in equation A1 and the MPEs are presented in Table A1.

For *photochemical damage*, the maximum permissible radiant power through the pupil (in watts), for $400 \text{ nm} < \lambda < 600 \text{ nm}$ and for $0.7 \text{ seconds} < t < 10^4$ seconds, can be equated as:

$$MPE_{\text{photochemical}} = \{100 \times C_B\} \Omega \left(\frac{A_{p,7}}{P} \frac{1}{T} \right), \quad (A2)$$

where the term in curly brackets is the ANSI-limiting integrated radiance of the circular source ($\text{J} \cdot \text{cm}^{-2} \cdot \text{sr}^{-1}$; ANSI Table 5b⁵), and again the term in parentheses is the conversion to radiant power through the pupil. The parameter P is always 5.44, since $\lambda < 600 \text{ nm}$ and $t > 0.7$ seconds. The other parameters are:

Ω = the solid angle of the source ($\Omega = \alpha^2 10^{-6}$ for the square source and α is in millirads).

C_B = a wavelength-dependent ANSI parameter that mimics the inverse of the action spectrum of photochemical damage: $C_B = 1$ for $\lambda < 450 \text{ nm}$, and $C_B = 10^{0.02(\lambda - 450)}$ for $450 \text{ nm} < \lambda < 600 \text{ nm}$ ($C_B = 229.1$ for 568 nm).

$A_{p,7}$, α , t are the same as for the thermal case. The photochemical limits are calculated by substitution of all relevant parameters in equation A2, and the MPEs are presented in Table A1.

A second simulation, that more closely addresses the pulsed nature of the exposure by an SLO with a galvanometer scanner was also considered.⁴² Let the frame rate be F Hz, and the number of raster lines used for imaging be R . In essence, it consists of the exposure of a segment of a raster line with length $\alpha_s = 2\alpha FR t_{\text{min}}$ (distance traveled during the confinement duration t_{min} for a galvanometer driven SLO) and width the minimum size associated with the Standard (α_{min}).⁵ This segment is traversed by $m = \alpha_{\text{min}} R / \alpha$ raster lines during each frame (assuming the line spacing of the SLO is smaller than α_{min} , as it usually is), and this occurs n times ($n = FT$) during the total exposure (in this study $T = 900$ seconds). If the return beam blanking of the galvanometer scanner is removed, then

m must be increased by a factor 2. The ANSI Standard recommends the use of three rules to assess the safety of repetitive pulsed exposure. The rule predicting the lowest level is the limiting level. Rule 1 checks that a single pulse in the simulation is below the MPE for $t = t_{\min}$. Rule 2 checks that the average power for the group of pulses is no higher than a single pulse over the entire size and duration. This rule is equivalent to the thermal and photochemical limits described by equations A1 and A2. Rule 3 (thermal) limits the exposure to a peak power that is (total number of pulses)^{-0.25} times lower than the limiting peak power for a single pulse ($t = t_{\min}$). For an SLO, rule 3 will always be lower than rule 1. The limiting peak power for Rule 3 in this simulation (or beam power with either no blanking or blanking depending on m) is then given by equation A3:

$$MPE_{\text{peak, rule 3}} = \frac{1}{(nm)^{0.25}} 6.93 \times 10^{-4} \frac{C_A C_E^*}{P t_{\min}^{0.25}}, \quad (A3)$$

where C_A is as above, $t_{\min} = 18 \mu\text{s}$, $P = 1$ ($t < 0.07$ seconds). C_E^* is a scaling factor for the rectangular line segment and is C_E (for a circular field) multiplied by the ratio of areas of the rectangular field to a circular field.⁴² Thus, $C_E^* = 8\alpha_s / [\pi(\alpha_s + \alpha_{\min})]$. After substitution and rearrangement, one obtains the MPE for a galvanometer SLO with no blanking of the back scan:

$$MPE_{\text{peak, rule 3}}(W) = 4.94 \times 10^{-7} R^{0.75} \frac{C_A \alpha^{1.25} F^{0.75} T^{-0.25}}{(1 + 2.4 \times 10^{-5} \times R \alpha F)}. \quad (A4)$$

This is the limit for the peak power in the simulation or the laser power at the pupil. Results for the MPE average power are calculated and given in the Table A1 for the AOSLO with $R = 512$ raster lines and $F = 27$ Hz.

The ANSI Standard was developed for the human eye with a focal length of ~17 mm. However, the focal length of the macaque eye is smaller (~15 mm). Assuming that the ma-

caque retina is equally sensitive to damage as the human retina, we correct for the shorter eye by multiplying the MPE by the ratio of the focal lengths squared. Thus, the above MPE equations are multiplied by $(15/17)^2$ to give the final MPEs for the macaque eye.

Section 8.2 of the ANSI standard allows for simultaneous exposures to multiple wavelengths; exposures from several wavelengths in the same time domain are additive on a proportional basis of spectral effectiveness. Thermal and photochemical limits are assessed separately.⁴² First, the MPE must be determined for each wavelength (Table A1). Exposure safety is achieved when the sum of the ratios of exposure power to the corresponding MPE for each wavelength is < 1 ,⁵⁹ or:

$$\sum_i \frac{E_i}{MPE_i} \leq 1, \quad (A5)$$

where the index i represents the different wavelengths. Since the powers of the 830- and 904-nm lasers are nearly constant in all experiments (225 and 70 μW , respectively), we determine the maximum power E_{568} of the 568-nm laser that would cause the above summation to be 1 – the safety limit). Using the MPEs for a $1/2^\circ$ square area and a 900-second exposure (Table A1), we find for the thermal limit:

$$E_{568} = \left(1 - \frac{225 \mu\text{W}}{627 \mu\text{W}} - \frac{70 \mu\text{W}}{883 \mu\text{W}} \right) \times 134 \mu\text{W} = 75 \mu\text{W}. \quad (A6)$$

Thus, when the two additional lasers are considered, the thermal MPE for the 568 nm laser is reduced from 134 to 75 μW . Photochemical damage only considers wavelengths shorter than 600 nm. Because only the 568-nm laser meets this criterion, the photochemical limit remains unchanged (107 μW). The limiting MPE is now the thermal limit (75 μW), but that change cannot explain the discrepancies between the MPE limits and the exposures causing damage observed in this study.